RSC Advances

PAPER

View Article Online
View Journal | View Issue

Cite this: *RSC Adv.*, 2016, **6**, 76390

Attaching folic acid on hydroxyapatite nanorod surfaces: an investigation of the HA–FA interaction

Marcelo Fernandes Cipreste,[a] Ismael Gonzalez,[a] Thaís Maria da Mata Martins,[b] Alfredo Miranda Goes,[c] Waldemar Augusto de Almeida Macedo[a] and Edésia Martins Barros de Sousa*[a]

Received 30th May 2016
Accepted 29th July 2016

DOI: 10.1039/c6ra14068h

www.rsc.org/advances

Hydroxyapatite (HA) nanostructures have attracted attention due to their great biocompatibility, bioactivity, osteoconductivity and good adherence to bone tissues and osteosarcoma cells, making possible the therapeutic replacement and reconstruction of bone matrix after tumor treatment. However, suitable surface modification is essential to enable the final performance of these materials. This paper describes the synthesis of HA nanorods and a route of functionalization of the HA surface with folic acid (folate). The samples were characterized by XRD, FTIR, TGA, CHN, XPS, BET, SEM and TEM in order to estimate the physical–chemical properties of the nanoparticles, such as morphology, size distribution, pore and surface parameters, and the stability of hydroxyapatite and folate interactions was systematically evaluated. In addition, an *in vitro* preliminary assay was conducted in order to investigate the biocompatibility of these systems in fibroblast cells. The results indicate that mesoporous hydroxyapatite nanorods around 70 nm were successfully synthesized with pure crystalline phase and folate can be strongly linked to hydroxyapatite nanorod surfaces following the methodology proposed in this work. In addition, this material shows great biocompatibility, presenting cell proliferation as an intrinsic characteristic, making this system suitable for the suggested biomedical applications.

1 Introduction

Bionanomaterials have been widely exploited in biomedical research due to the large range of applications they can provide. Among them, hydroxyapatite (HA), chemically defined as $Ca_{10}(PO_4)_6(OH)_2$, has attracted much attention due to its similarity to the bone mineral phase and crystalline structure, showing great biocompatibility, bioactivity[1–3] and osteoconductivity.[1,4] HA nanorods can present good adherence to bone tissues and osteosarcoma cells, making possible the therapeutic replacement and reconstruction of bone matrix after tumor treatment.[4] However, in order to obtain synthetic HA nanorods similar to the bone material, it is very important to study how their properties change with the dimensions and chemical surface of the nanoparticles.

Regarding the dimensions, the size range of the particles is a very important feature for cancer treatment materials, considering its spontaneous accumulation in tumor cells. Nanomaterials show enhanced permeability and retention, known as EPR effect, on tumor tissues due to the enlarged porosity of tumor vessels,[5] generally in nanoscale,[5] and poor lymphatic drain,[6] making possible the preferential accumulation of the nanoparticles in tumor sites and avoiding their accumulation on healthy tissues. These characteristics make bionanostructures candidates for a passive targeting strategy to act as drug delivery systems for controlled chemical release or radioisotopes carrier systems,[7–10] with selective action on tumor sites.

In the case of chemical surface, the performance of bionanomaterials in tumor targeting strategy depends directly on its great binding rates on cancer cells and this feature can be achieved by the functionalization process of nanoparticles.[11] Then, a suitable surface modification is essential to allow an adequate performance of these materials. The functionalization processes of nanomaterials can improve physicochemical characteristics of nanoparticles surfaces while maintaining its bulk characteristics.[12] One of these features is to allow the active accumulation on tumor sites due to the system of ligand–receptor interactions that induce receptor-mediated endocytosis and internalization inside the cells.[5] Effective binding and internalization requires that receptors are overexpressed exclusively on cancer cells membrane,[5] consisting in active targeting strategy.

Over the past decade or so, folic acid (folate – FA) receptor functionalization process in different inorganic nanostructure

[a]*Centro de Desenvolvimento da Tecnologia Nuclear – CDTN, Avenida Presidente Antônio Carlos, 6.627-Campus UFMG, CEP 31270-901, Belo Horizonte, Minas Gerais, Brazil. E-mail: sousaem@cdtn.br; Fax: +55 3130693164; Tel: +55 3130693223*

[b]*Universidade Federal de Minas Gerais, Instituto de Ciências Biológicas, Departamento de Morfologia, UFMG, Belo Horizonte, Brazil*

[c]*Universidade Federal de Minas Gerais, Instituto de Ciências Biológicas, Departamento de Bioquímica e Imunologia, UFMG, Belo Horizonte, Brazil*

has receive much attention as it is overexpressed in osteosarcoma cells and can facilitate the uptake of nanoparticles in this kind of cell.[11] Studies concerning to the conjugation of HA nanorods with FA have been reported but almost all of these works involve the use of a polymeric micelle for HA coating or a polymer ligand and a posterior process of conjugation with HA, leading to complex chemical routes and materials.[13–15] More recently, Lafarga *et al.* (2015)[16] showed that HA functionalized with folate without a polymer ligand presented lower oxidative stress than pure hydroxyapatite in an *in vivo* experiment. Despite many years of experimental synthesis, characterization, and increasing use of HA in different applications, to the best of our knowledge, relatively few works[14–16] actually address the investigation of the HA–FA as a nanoplatform for bioapplications and no deep investigation of the stability and nature of this chemical bond were studied yet.

In view of the aforementioned, in the present work we investigate the functionalization strategy of HA nanorods with folate and a systematic study on the structural properties of hybrid samples and the chemical interaction between folate and hydroxyapatite nanorods surfaces were performed. For this proposal, two systems composed of hydroxyapatite nanorods functionalized with folate without linking to a polymer micelle were synthesized and characterized by XPS, FTIR, CHN, TGA and XRD techniques in order to study the interaction stability of HA and FA. The biocompatibility in fibroblasts cells was also preliminary tested to verify if the functionalized hydroxyapatite nanorods is a great candidate to act as a drug delivery system or radioisotope carrier for osteosarcoma end bone metastases treatment and diagnosis.

2 Materials and methods

2.1 Synthesis of hydroxyapatite nanorods (HA)

Hydroxyapatite nanorods were prepared by surfactant-assisted hydrothermal method with some modifications in accordance with the published procedure.[17,18] Calcium nitrate tetrahydrate, $Ca(NO_3)_2 \cdot 4H_2O$, potassium phosphate dibasic trihydrate, $K_2HPO_4 \cdot 3H_2O$, and CTAB (hexadecyltrimethylammonium bromide) were purchased from Sigma-Aldrich with no further purification. The present method consisted in the preparation of two precursor solutions of calcium and phosphate, solution (I) and (II) respectively. The preparation of solution (I) started with the complete dissolution of CTAB (2 g) in 150 mL Milli-Q® water to promote micelles formation, followed by dissolution of calcium nitrate tetrahydrate (0.167 M); this solution was kept under stirring for 6 hours to promote self-assembly of calcium ions on the CTAB micelles. Solution (II) was prepared by the complete dissolution of potassium phosphate dibasic trihydrate (0.1 M) in 150 mL Milli-Q® water. The pH of both solutions was adjusted to 12 with NaOH (Sigma-Aldrich). The next step consisted in the slowly addition of solution (II) in the solution (I) using a motor-driven burette (TITRONIC® universal, USA) under vigorous stirring. The resultant suspension was kept under stirring overnight in a hydrothermal reactor during 10 hours at 100 °C. The filtered powder was dried during 24 hours and calcined at 600 °C during 6 hours to promote CTAB removal, resulting in a fine white powder.

2.2 Functionalization process with folic acid

Two methods of HA functionalization with folic acid were used to evaluate the surface modification: the direct functionalization of HA with folate (HA–FA) and the functionalization process with aminated folate (HA–FA_{NH_2}). The functionalization process of HA with FA was carried out by mixing a 1 : 2 molar proportion of HA and folate (Sigma-Aldrich) in Milli-Q® water and keeping under vigorous stirring during 24 hours at 50 °C in reflux system. The resulting yellow powder was collected under vacuum filtration and dried at 37 °C during 24 hours. The second functionalization method followed the amination process of folate described by Pan *et al.* (2013)[13,] and Lee *et al.* (2003)[19] with minimal modifications. In the first step folic acid (1 mmol) (Sigma-Aldrich) was dissolved in 30 mL of dimethylsulfoxide (DMSO) (Sigma-Aldrich) and 1.2 mmol of 1-ethyl-3-(3-dimethylaminopropyl) carbodiimide hydrochloride, EDC, (Sigma-Aldrich). Then, 2 mmol of *N*-hydroxysuccinimide, NHS, (Sigma-Aldrich) were added to the solution with stirring during 6 hours at 50 °C in reflux system. In the second step 10 mmol of ethylenediamine (Sigma-Aldrich) was added in the solution and allowed to react with stirring overnight. The chemical reaction of folate amination is represented on Scheme 1. This material was dried at room temperature during 24 hours. The functionalization process of HA with FA_{NH_2} was carried out by mixing a 1 : 2 molar proportion of HA and aminated folate in Milli-Q® water and keeping under vigorous stirring during 24 hours at 50 °C in reflux system. The resulting yellow powder was washed with acetone and Milli-Q® water under vacuum filtration system and was dried at 37 °C during 24 hours.

2.3 Hydroxyapatite–folate interaction stability assay

The stability of the chemical interactions between hydroxyapatite nanorods and folate group was investigated by the assessment carried out in simulated body fluid (SBF) in different times. The test consisted in the preparation of 1 mg mL^{-1} suspensions of HA–FA and HA–FA_{NH_2} in SBF with pH 7.3. These

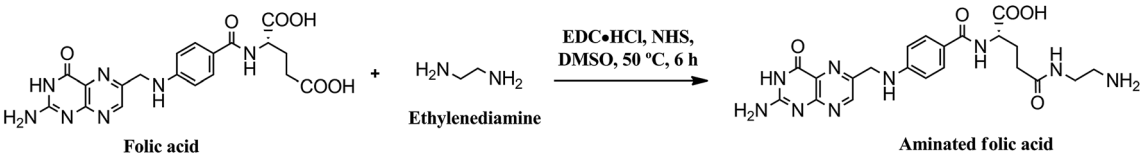

Scheme 1 Representation of chemical reaction of folate amination.

suspensions were incubated and kept under 50 rpm at 37 °C during variable time intervals (2, 8, 24 and 48 hours). After each incubation time, the suspensions were filtered by swinex systems with 200 nm pore membrane (Millipore®), and the powders were investigated by CHN elemental analysis.

2.4 Characterizations

The crystalline phases of synthesized HA nanorods were evaluated by X-ray diffraction (XRD-Rigaku Inc., Japan) with Cu Kα radiation ($\lambda = 0.154$ nm) in which data were collected from 10° to 80° (2θ) with a step size of 1° min^{-1}. Fourier transform infrared spectra (FTIR-Nicolet 6700, Thermo Scientific, USA) were recorded in the range of 4000–400 cm^{-1} with 4 cm^{-1} resolution and 64 scans to evaluate the chemical composition of the samples and to investigate the functionalization process efficacy; the samples were prepared in KBr (Sigma-Aldrich) powder. To investigate the thermal stability of HA and the weight losses associated with folate on functionalized samples, thermogravimetric analyses (TGA-DTG-60H, Shimadzu, Japan) were carried out under nitrogen atmosphere from room temperature to 700 °C. CHN elemental analyses (CHN – 2400, PerkinElmer, USA) were performed to investigate the presence of folate on functionalized samples by the analysis of carbon and nitrogen levels. X-ray photoelectron spectroscopy analysis (XPS – Specs Phoibos 150 electron analyzer) was carried out to investigate the HA surface and the interactions between HA and FA, using monochromatized Al Kα radiation (1486.6 eV) at a power of 350 W. An electron flood gun, operated at 0.1 μA, was used to compensate the charge effect in the samples. The C 1s core level at 284.6 eV was used as reference for the calibration of the binding energies (BE) of different elements. The porosity parameters were evaluated by N_2 adsorption analysis (Autosorb iQ-Quantachrome, EUA). The non-functionalized samples were outgassed during 2 hours at 300 °C and the functionalized samples were outgassed during 48 hours at 40 °C; the specific surface area was calculated by the traditional method of Brunauer, Emmett and Teller (BET). Particle size and morphology analyses were evaluated by transmission electron microscopy (TEM-Tecnai G2-12 SpiritBiotwin, FEI Company, Japan) and scanning electron microscopy (SEM – Σigma VD series, ZEISS, Germany).

2.5 Preliminary biocompatibility assay

Biocompatibility of the systems was preliminary tested by the MTT (3-(4,5-dimethylthiazol-2-yl)-2,5-diphenyl tetrazolium bromide) (Sigma-Aldrich) viability assay[20] in a primary fibroblasts cells. Human eyelid skin was used to isolate fibroblasts following Martins *et al.* (2014)[21] methodology. All samples were collected after obtaining informed consent from the patients according to procedures approved by Ethics Committee of the Universidade Federal de Minas Gerais (no. ETIC 02887512.6.0000.5149). All experiments were performed in compliance with resolution 466/12 of the Brazilian National Health Council (CNS) published on December 12, 2012.

The cells were cultivated in DMEM (Dulbecco's Modified Eagle Medium) (Sigma-Aldrich) with 10% of fetal bovine serum (Sigma-Aldrich) in a CO_2 atmosphere at 37 °C and then were added in a 24 wells plate (1.0×10^4 cells per well), with 6 blank wells and 3 control wells. The plates were left in a CO_2 atmosphere at 37 °C during 24 hours and them the cells were treated with the materials in five concentrations (0.5, 5, 25, 50 and 100 μg mL^{-1}) and incubated at same conditions during 48 hours. After the incubation period, the wells contents were removed and washed with phosphate-buffered saline (PBS) followed by the addiction of 170 μL of MTT (0.5 mg mL^{-1}) and 210 μL of DMEM per well. The plates were incubated in a CO_2 atmosphere at 37 °C during 2 hours and the formazan crystal formation were observed in a microscope. 210 μL of sodium lauryl sulfate (Sigma-Aldrich) 10% HCl were added per well and the plates were incubated in a CO_2 atmosphere at 37 °C overnight. After 18 h, 100 μL of each well were transferred in triplicate to a 96 well plate and the absorbance was red at 570 nm with a microplate reader (Multiskan GO, Thermo Scientific, USA).

3 Results and discussions

3.1 X-ray diffraction (XRD)

The XRD pattern of the synthesized hydroxyapatite is shown on Fig. 1, which reveals a single phase formation of hexagonal HA with $P63/m$ space group. Characteristic peaks in Bragg angle (2θ) of approximately 32°, 33° and 34° that can be assigned to (211), (300) and (202) reflections respectively (JCPDS files: 09-0432) confirm the formation of a pure crystalline structure matching the same results found in literature.[22–24] This analysis indicates that the presence of CTAB cannot induce the crystallization of any other crystallographic phases. The X-ray diffraction patterns for HA–FA and HA–FA_{NH_2} are also shown on Fig. 1 and they are similar to the non-functionalized sample, suggesting that no other crystalline phase was formed in these functionalization processes.

X-ray diffraction data were also used to estimate the crystallite size of the HA, HA–FA and HA–FA_{NH_2} samples (17.3 ± 5

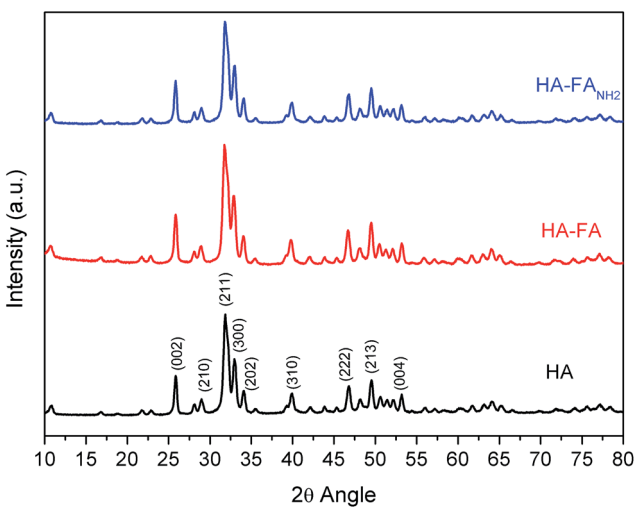

Fig. 1 X-ray diffraction pattern for HA, HA–FA and HA–FA_{NH_2} samples.

nm, 15.7 ± 5 nm and 16.7 ± 5 nm, respectively) following Scherrer equation:

$$D = K\lambda/\beta_{size}\cos\theta$$

where D is the crystallite size, $K = 0.9$ for spherical shape, λ is the radiation wavelength (1.5418 Å for Cu Kα), β_{size} is the size contribution to full width at half-maximum (FWHM) of the reflection peaks, and θ is the diffraction angle based on the mean peak of HA (211). As expected, HA sample presents a small crystallite size at around 17 nm; this size is an important feature of this material that indicates its suitability for use as theranostic system useful in therapeutic of anti-tumor treatment. Similar results were observed for functionalized samples, since that a small decrease in the size observed could be attributed to the intrinsic characteristic of the measurement method. So, no transformation in the nucleation and growth processes of hydroxyapatite sample during the surface modification occurs, considering that these functionalization processes did not follow an *in situ* method.

3.2 Fourier transform infrared spectra (FTIR)

FTIR spectra were acquired to confirm the composition of HA sample and the functionalization process of this sample with amino group (–NH_2) and FA. Fig. 2 illustrates these results. All samples present the characteristic vibrational modes bands of HA, in agreement with the literature.[17,25,26] The two peaks at 961 cm^{-1} and 1036 cm^{-1} corresponds to $\nu1$ and $\nu3$ phosphate stretching modes while the peak at 473 cm^{-1} and the strong peaks at 565 and 604 cm^{-1} point the presence of $\nu2$ and $\nu4$ phosphate bending modes.[17] The OH peaks could be observed at 3569 and 631 cm^{-1}.[25] The broad band observed from 3237 to 3663 cm^{-1} could be attributed to H_2O vibration modes.[3] The peaks observed at 1418 and 1479 cm^{-1} could be attributed to the presence of CO_3^{2-}, suggesting the formation of carbonated hydroxyapatite.[27] This carbonate phase could be formed in calcination process due to the evaporation of CTAB causing chemical reaction between C and O_2, since this process was not conducted in inert atmosphere. FTIR spectra of HA–FA and HA–FA_{NH_2} samples suggest the presence of folate on these functionalized samples by the comparison with the matching bands (hatched rectangle) relative to FA spectrum. Fig. 2 also exhibits the characteristic IR absorption peaks of FA at 1605 cm^{-1} (benzene, conjugated double absorption), 1697 cm^{-1} (amide), and 1481 cm^{-1} (hetero-ring, conjugated double bond).[28] The transmittance band at 1645 cm^{-1}, representing NH bend, is also a strong evidence of the primary amine group,[29] although it is not possible to identify clearly this band because some vibration modes occurred in the same frequency interval of the bands cited above.

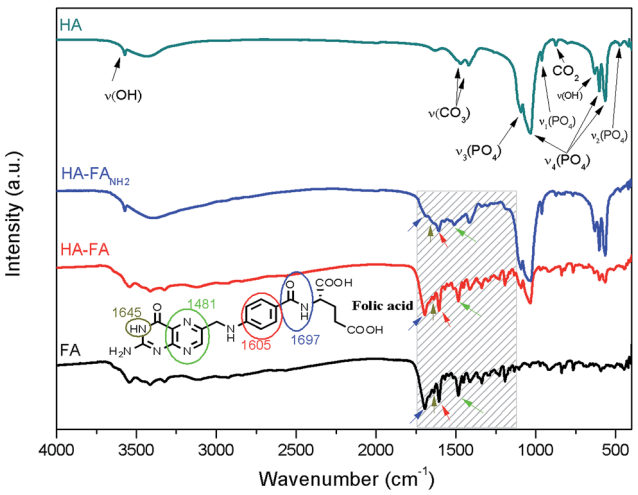

Fig. 2 FTIR spectra collected for HA, HA–FA, HA–FA_{NH_2} samples and FA.

3.3 Thermogravimetric analysis (TGA)

TGA analysis was performed in order to study the thermal stability of the synthesized hydroxyapatite nanorods during heat treatment and to investigate the functionalization process with folate by analyzing the degradation of organic material. The weight losses of all samples were evaluated in the range of 25 to 700 °C and are shown in Table 1. Fig. 3 represents TGA curves of the synthesized samples where it could be observed the high stability of HA nanorods during the whole heat treatment in perfect agreement with the literature.[23,25] It is observed a small weight loss up to 150 °C attributed to the removal of interstitial water from the sample. TGA curve of the HA–FA sample shows a significant weight loss of about 42% around 150 °C up to 700 °C that might be due to the degradation of folate. In case of the HA–FA_{NH_2} sample, the curve shows an 8.6% weight loss of the respective initial masses in the same temperature range. It may be associated with the degradation of the FA_{NH_2} chains anchored on HA surface.

This important difference could suggest that in the HA–FA samples a higher amount of folate group is anchored in the HA surface. Also, this variation could be a consequence of different kinds of folate interactions with HA in the two functionalization methods. Indeed, Table 1 shows a weight loss of 5.9% from 150 to 250 °C for HA–FA and there is no significant weight loss in this range for HA–FA_{NH_2} sample. This difference is apparently due to a weak interaction between HA surface and non-aminated folate, aspect which will be further discussed with the CHN and XPS analysis.

3.4 CHN elemental analysis (CHN)

Since the functionalization of the HA nanorods involves the anchorage and the interaction of organic functional groups on

Table 1 Weight losses in TGA and CHN elemental analysis[a]

	Weight losses (%)			Elemental analysis	
Sample	40–150 °C	150–250 °C	250–700 °C	Carbon (%)	Nitrogen (%)
HA	1.3	0.3	0.5	0.9	0.1
HA–FA	5.0	5.9	36.1	36.5	15.6
HA–FA_{NH_2}	2.2	0.5	8.1	5.7	2.8

[a] Related error: 0.3%.

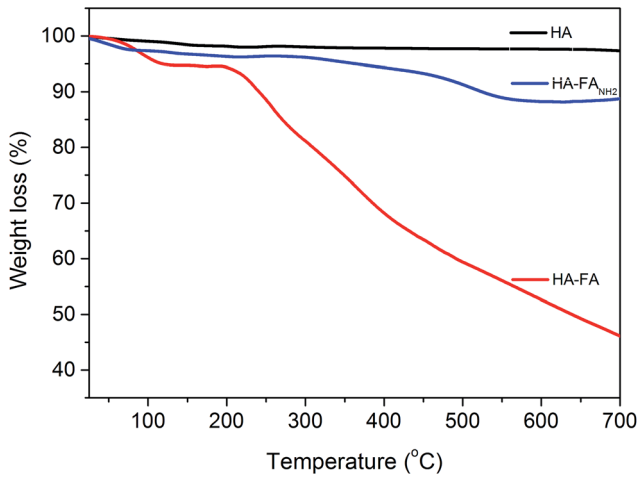

Fig. 3 Thermogravimetric assay of HA, HA–FA and HA–FA$_{NH_2}$ samples.

the HA surface, CHN elemental analysis is an important tool to estimate the success of the functionalization process. Results of CHN analysis obtained for the synthesized samples are shown in Table 1. These results indicate that HA sample contains carbonate ions, in agreement with FTIR results, due to the percentage (0.9%) of carbon found on this sample. The increasing amount of carbon from HA to HA–FA and HA–FA$_{NH_2}$ (0.9% to 36.5% and 5.7% respectively) and the presence of nitrogen in the HA–FA and HA–FA$_{NH_2}$ functionalized samples (15.6 and 2.8%, respectively) suggest the presence of folate on the samples surface, reinforcing the indicative of the efficient functionalization processes. These results are in agreement with the TGA analysis, evidencing that there is a higher deposition of folate on HA–FA indicating a higher amount of functionalization group in this sample compared to the results obtained for the HA–FA$_{NH_2}$ sample.

In order to evaluate the relationships between the amounts of nanorods and organic groups during functionalization process, results of CHN and TGA were used to calculate the relations for folic acid and aminated folic acid grafted on HA nanorods. These results (Table 2) show that the HA–FA sample has consistently greater amounts of organic group (70.4 g FA/100 g HA), and for the case of HA–FA$_{NH_2}$ sample, a lower amount of organic group than the corresponding HA was observed (9.4 g FA$_{NH_2}$/100 g HA). These results reinforce that a higher deposition of folate occur on HA–FA sample. The differences observed on carbon and nitrogen content between these samples will be further discussed by hydroxyapatite–folate interaction stability assay and XPS analysis.

3.5 Hydroxyapatite–folate interaction stability assay (I.S.A.)

The interaction force and the stability of FA and aminated FA on HA surface were investigated by analyzing carbon and nitrogen contents by CHN elemental analysis as proposed on methodology, results are shown in Table 2.

As it could be seen, carbon and nitrogen percentages drastically decrease for HA–FA sample the first 2 hours of test (36.5% to 21.7% and 15.6% to 9.0%, respectively) and continue to decrease up to 48 hours. No significantly decreases in carbon and nitrogen amounts could be observed for HA–FA$_{NH_2}$ sample from 2 hours up to 48 hours, indicating a great stability of interaction between aminated folic acid and hydroxyapatite nanorods. The final results show a weight loss of 79% and 19% of functionalized moieties in the HA–FA and HA–FA$_{NH_2}$ respectively. The anchored mass amounts presented on Table 2 also indicate the same tendency. After 2 hours of incubation, HA–FA sample lost 29.3 g/100 g HA while HA–FA$_{NH_2}$ lost only 0.4 g/100 g HA; after 48 hour of incubation, HA–FA sample lost 57.7 g/100 g HA while HA–FA$_{NH_2}$ lost only 2.2 g/100 g HA in terms of accumulative amount. So, it is possible to infer that the functionalization process with aminated folic acid resulted in a more stable material when compared with non-aminated folic acid functionalization process, and this hypothesis is supported by the XPS results.

3.6 X-ray photoelectron spectroscopy (XPS)

XPS analysis was conducted to investigate the chemical composition of the nanoparticles surfaces in order to study the nature of folate interaction with HA. The XPS survey spectra shown in Fig. 4 indicates that the surface of the HA sample is

Table 2 CHN elemental analysis results of functionalization stability tests and relative mass calculations

Sample	Carbon (%)	Hydrogen (%)	Nitrogen (%)	FA mass (g/100 g HA)	ΔFA mass[a]	FA moles (mol/100 g HA)
HA	0.9	0.3	0.1	—	—	—
HA–FA	36.5	3.7	15.6	70.4	—	0.159
HA–FA I.S.A.-2H	21.7	2.5	9.0	41.1	29.3	0.093
HA–FA I.S.A.-8H	15.4	2.7	5.4	28.7	41.7	0.065
HA–FA I.S.A.-24H	7.7	1.0	3.1	13.4	57.0	0.030
HA–FA I.S.A.-48H	7.3	1.0	2.4	12.7	57.7	0.028
HA–FA$_{NH_2}$	5.7	0.9	2.8	9.4	—	0.019
HA–FA$_{NH_2}$ I.S.A.-2H	5.5	1.0	2.3	9.0	0.4	0.018
HA–FA$_{NH_2}$ I.S.A.-8H	5.1	0.8	2.2	8.2	1.2	0.017
HA–FA$_{NH_2}$ I.S.A.-24H	5.0	0.8	2.0	8.0	1.4	0.016
HA–FA$_{NH_2}$ I.S.A.-48H	4.6	0.7	2.0	7.2	2.2	0.015

[a] ΔFA = (FA mass on HA–FA sample) – (FA mass on HA–FA I.S.A.-*X*H). Related error of measurements: 0.3%.

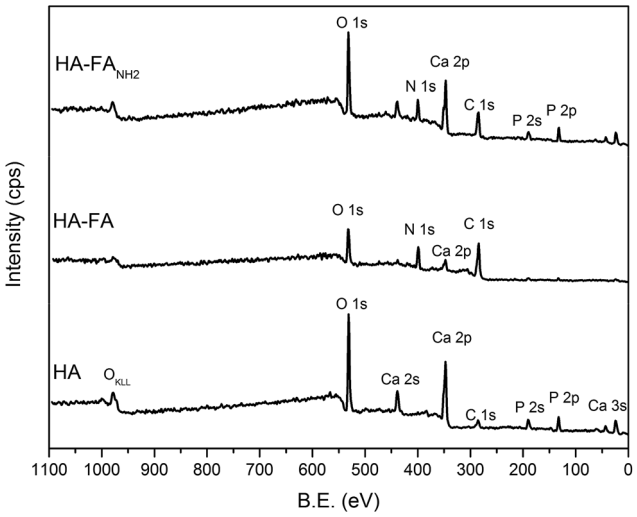

Fig. 4 XPS survey spectra for HA, HA–FA and HA–FA$_{NH_2}$ samples.

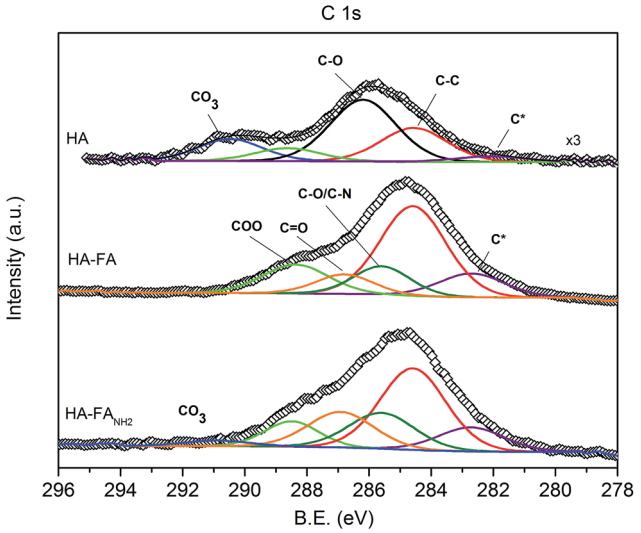

Fig. 5 XPS spectra of C 1s photoelectron peaks of the synthesized samples.

constituted only by O, Ca, C and P. The carbon in HA corresponds to carbonate ions present in the structure of the sample, as previously evidenced by FTIR, in addition to some surface carbon contamination (carbon adventitious) normally detected in XPS analysis. Nitrogen is present in the functionalized samples, as expected. An increase of the C and N concentration as well as the decrease of Ca and P in samples HA–FA and HA – evidences the incorporation of folate to the samples surface. In agreement with TGA and CNH analysis, the XPS results indicate a higher incorporation of folate in the HA–FA sample. Table 3 shows the concentration of the elements present in the sample surfaces, as obtained by XPS.

Fig. 5 shows the C 1s XPS spectra of the synthesized samples. A fitting procedure was used to determine the different contributions to the 1s core level of C. For the HA nanoparticles, the component at 284.6 eV corresponds to C–C bonds, and the components at 286.2 and 288.6 eV correspond to CO_x species, suggesting that CTAB was not completely removed after calcination process. The additional component at 290.5 eV is attributed to the presence of carbonate ions (CO_3^{2-}), as previously mentioned. For the HA–FA and HA–FA$_{NH_2}$ samples, it is possible to observe an enhanced intensity of C–C and three new components at 285.6, 288.6 and 288.4 eV, corresponding to nitrogen/oxygen bonded carbon (C–O/C–N), carbonyl carbon (C═O) and carboxyl carbon (COO), respectively. These spectral contributions are characteristic of the organic structure of the folate and of the functional groups present in the functionalized samples.[30] CO_3^{2-} is not detected in the functionalized samples. Furthermore, the small spectral component at low BE (282 eV) is assigned to some carbon with a differential charging effect (*C**) in the sample surface. This phenomenon is frequently observed in the Si, O and C photoelectron spectra from materials with very low electrical conductivity, as ceramics.[31]

Table 3 Surface elemental analysis obtained by XPS

Sample	Core level	B.E. (eV)	% At
HA	O 1s	531.7	49.4
	C 1s	285.7	13.4
	Ca 2p	348.3	22.6
	P 2p	134.3	14.6
HF–FA	O 1s	532.0	20.9
	C 1s	284.8	57.6
	Ca 2p	348.1	4.1
	P 2p	134.1	2.6
	N 1s	400.0	14.8
HA–FA$_{NH_2}$	O 1s	530.2	40.8
	C 1s	284.8	21.4
	Ca 2p	347.2	17.8
	P 2p	132.4	13.6
	N 1s	400.3	6.5

It should be also pointed out that a significant chemical shift is observed in the XPS spectra of Ca 2p and P 2p core levels of the HA–FA$_{NH_2}$ sample, when compared with HA nanoparticles, and not for the HA–FA sample, as show in Fig. 6 (and also in Table 3). These chemical shifts suggest a possible interaction between Ca and P surface atoms with the folate that only occurs when the synthesis is carried out using the aminated FA, and also could explain why the sample HA–FA$_{NH_2}$ shows a very low folate release (higher stability) in the hydroxyapatite–folate interaction stability assay, as mentioned above.

The N 1s XPS peaks for HA–FA and HA–FA$_{NH_2}$ samples are shown in Fig. 7. In the spectra, it is possible to observe a low intensity component at 397.2 eV corresponding to N in aromatic rings and two predominant components at 399.2 and 400.3 eV that are assigned to amine and amide groups, respectively. For sample HA–FA$_{NH_2}$, the additional low intensity component at 401.8 eV, corresponding to a more electronegative chemical environment, could be related with the chemical shifts of the Ca 2p and P 2p peaks shown in Fig. 6.

The quantification of the different species of C and N on the surface of the functionalized sample surfaces, as determinate through the deconvolution of the C 1s and N 1s XPS peaks is summarized in Table 4. From the results, it is evident a higher

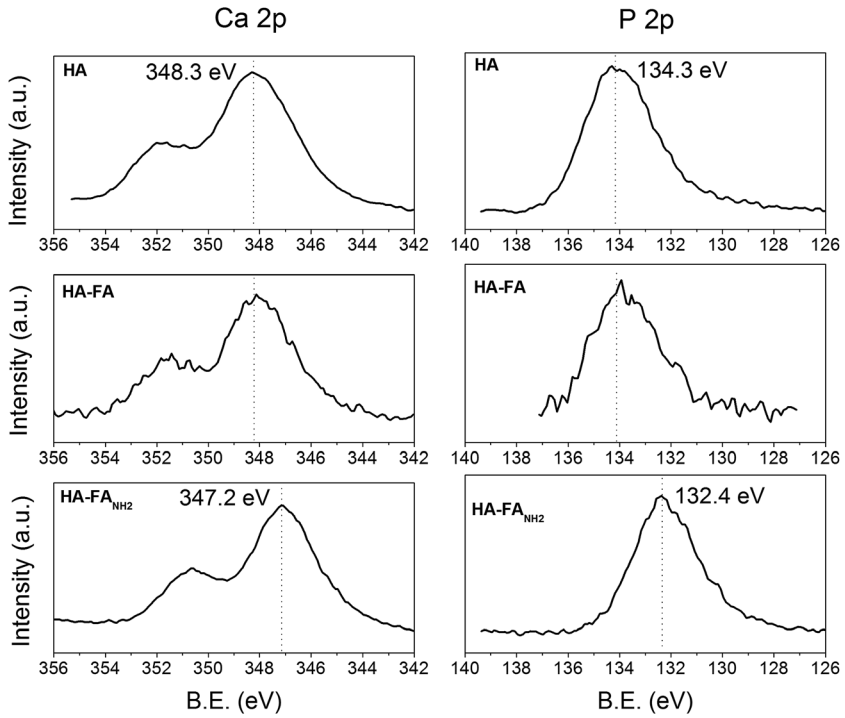

Fig. 6 XPS spectra for Ca 2p and P 2p photoelectrons peaks of the synthesized samples.

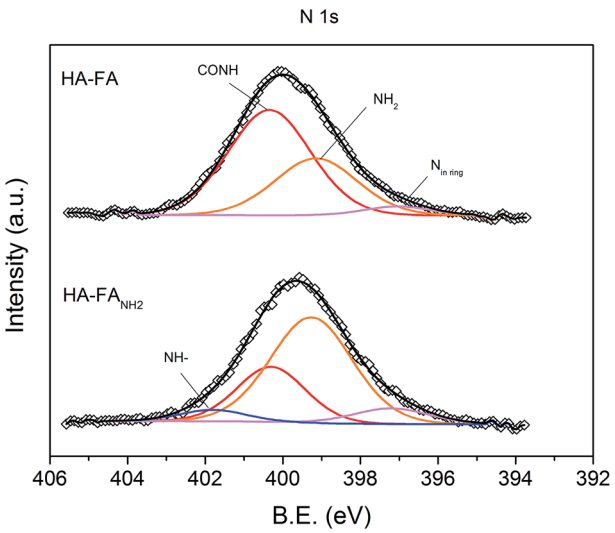

Fig. 7 XPS spectra of N 1s photoelectrons peaks of the HA–FA and HA–FA$_{NH_2}$ samples.

Table 4 C and N species on functionalized sample surface determinate by XPS

	HA–FA		HA–FA$_{NH_2}$	
C type	**BE (eV)**	**%**	**BE (eV)**	**%**
C–C	284.6	48.8	284.6	40.0
C–O/C–N	285.6	13.3	285.6	17.7
C=O	286.8	9.3	286.9	17.5
COO	288.4	15.6	288.5	10.2
CO_3^{2-}	nd	nd	290.9	2.8
N type	**BE (eV)**	**%**	**BE (eV)**	**%**
$N_{in\ ring}$	397.1	4.654	397.2	8.3
NH_2	399.2	34.62	399.3	60.2
CONH	400.4	60.726	400.3	26.3
NH–COCa/P	nd	nd	401.8	5.3

fraction of C–N and C=O species in the HA–FA$_{NH_2}$ sample in comparison with the HA–FA sample in which there is a higher fraction of COO species. Furthermore, it is also evident a considerable increment of NH_2 species and depletion of CONH species on sample. These results could be a consequence of the previous amination process of the FA, which not only provide higher formation of amine groups but also the formation of groups C=O due to the partial amination of the carboxyl groups.

As an organic material, folate tends to raise the carbon levels on functionalized materials taking over of the sample surface and, thus, avoiding the CO_3^{2-}, Ca and P photoelectrons to escape from the nanoparticles surfaces. However, our results (spectra in Fig. 6 and Table 3) show that Ca and P are still detected by XPS while the CO_3^{2-} is not detected. These results allow us to propose a possible preferential interaction of the folate with the CO_3^{2-} species present in the HA surface through the amine groups (NH–COCa/P), interaction that is strongly favored by the amination process. Since the CO_3^{2-} are linked to the Ca and P in the structural arrange of the HA, this interaction could justify the chemical shift observed for the Ca 2p and P 2p peaks. This kind of interaction is not common in ceramics bulks but must be reasonable in surface structures due to the reactive ions present on the HA surface.

Thus, the XPS results and the results from stability tests for HA–FA and HA–FA$_{NH_2}$ samples allow to infer that folate

interaction on surface of the functionalized samples occurs in two different ways, as shown in the schema in Fig. 8: (i) in the case of the HA–FA, it could occur majority as folate deposition in layers like core–shell structures, may be through a weak interaction as van der Waals forces which avoid folate keep on surface during release test in spite of the great amount incorporate to the surface. (ii) On the surface of HA–FA_{NH_2} predominates a stronger adsorption and more selective by a chemical interaction of folate through their amine with the CO_3^{2-} on surface (NH–COCa/P). This kind of interaction could suggest a more ordered folate anchorage on surface that could include folate molecules arranged perpendicularly to the surface (90°). Even when previous results indicate that the folate incorporation on the sample HA–FA_{NH_2} was considerably lower than in the sample HA–FA, this assumption is additionally supported by the increase of $N_{in\ ring}$ fraction in the N 1s peak (Table 4), which suggests a more superficial disposition of the double aromatic ring from FA as illustrated in Fig. 8.

Results from these characterizations indicate that the functionalization process of HA with aminated folic acid provides a more adequate material to act as drug delivery system or radioisotope carrier for biomedical applications due to the higher stability of hydroxyapatite–folate linkage. Considering this, the following experiments were conducted only with HA and HA–FA_{NH_2} samples.

3.7 Nitrogen adsorption analysis (BET)

Nitrogen adsorption and desorption isotherms of the samples are shown in Fig. 9. The isotherm of HA sample is classified as type III.[32] Note that the form of the isotherm is not affected by the process of functionalization, that shows the type-H3 hysteresis loop which is often observed with aggregates of plate-like particles that give rise to slit-shape pores For HA–FA_{NH_2} it could be observed a reduction of N_2 adsorption volume for all the relative pressures suggesting again that FA_{NH_2} functionalized the surface of the nanoparticles. Such difference might be attributed to the result of FA long chain molecules connected with amino groups.

Textural properties of HA and functionalized sample were estimated by the traditional method of Brunauer, Emmett and Teller (BET). A sensible difference was observed in the values of

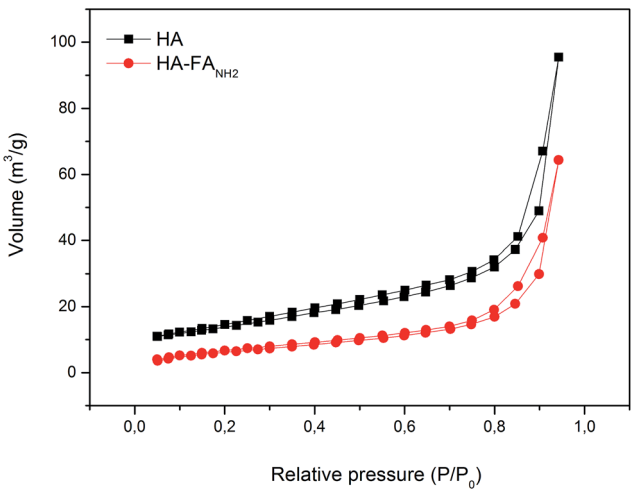

Fig. 9 Nitrogen adsorption and desorption isotherms.

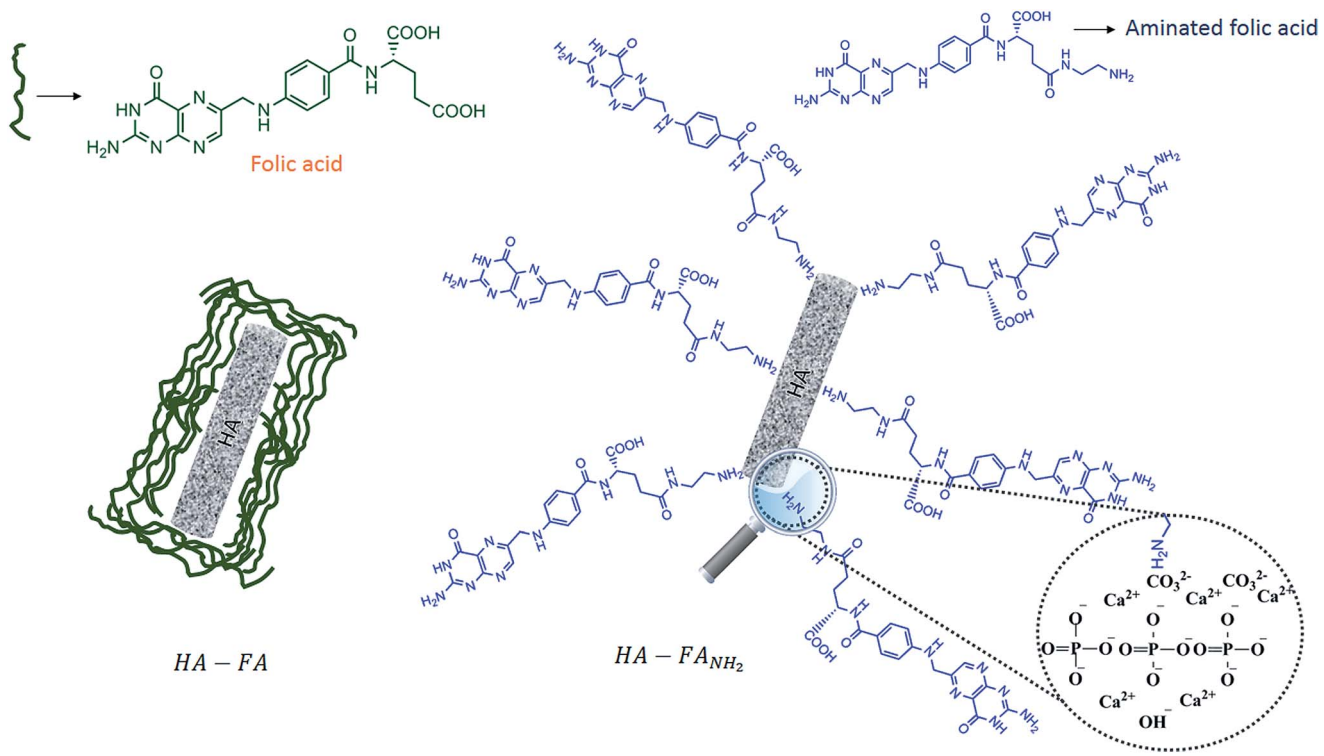

Fig. 8 Proposed scheme for HA nanorods functionalized with folate based on XPS results.

the surface area (49 m^2 g^{-1} for HA and 24 m^2 g^{-1} for HA–FA_{NH_2}) which may be an indication of the presence of functionalized moieties in the surface of HA. The total pore volume of HA–FA_{NH_2} (0.06 m^3 g^{-1}) was lower than the HA samples (0.09 m^3 g^{-1}), although no difference was observed in the pore diameter (18 nm for both samples). The measured pore diameter and pore volume are suitable for drugs and radioisotopes incorporation, making this system a great candidate to be used as a drug delivery system or radioisotope carrier for osteosarcoma treatment.

The occupied density by functionalizing was estimated from the amount of surface area found by BET, CHN and TGA results for HA–FA_{NH_2} sample. The result obtained is of 1 molecule/40 $Å^2$. This folic acid density on HA nanorods indicates that a large amount of molecules can be stably anchored at the nanoparticles surfaces, making possible to the system to be actively targeted to osteosarcoma cells.

3.8 Scanning electron microscopy (SEM) and transmission electron microscopy (TEM)

SEM micrograph of the HA samples are shown in Fig. 10. As it can be seen, the microstructure of the HA sample was observed as nanorods and the size distribution is relatively narrow (Fig. 10a). SEM technique also indicate that the presence of folate on the HA nanorods does not change the particle size and morphology of the samples (Fig. 10b). Fig. 10c shows the TEM image of HA samples, indicating a well-defined nanostructure. High resolution TEM image (Fig. 10d) indicates that HA nanorods are consisted of an arrangement of smaller nanocrystals, confirming the XRD measurements and calculations. Fig. 11 shows the particle size distribution estimated by Quantikov

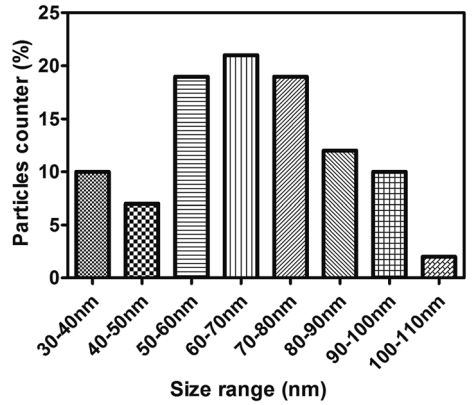

Fig. 11 Size distribution based on TEM images.

Image Analyzer software[33] indicating a mean particle size measuring from 60 to 70 nm. According to Torchilin[6] this size range is desirable in candidate nanomaterials to act in cancer treatment by the EPR effect because the accumulation of nanorods on tumor sites will be favorated by the nanoscale of the porosity of blood vessels that is common on tumors.

3.9 Biocompatibility tests

The cell viability test with MTT salt was conducted to investigate the biocompatibility of HA and HA–FA_{NH_2} on fibroblast cells, consisting of preliminary assay for biological designed materials. Due to the low stability of HA–FA nanorods according to CHN and HA–folate interaction stability assay, this sample was not evaluated in this assay. Drug delivery systems and radioisotope carries must represent no toxicity on healthy cells.

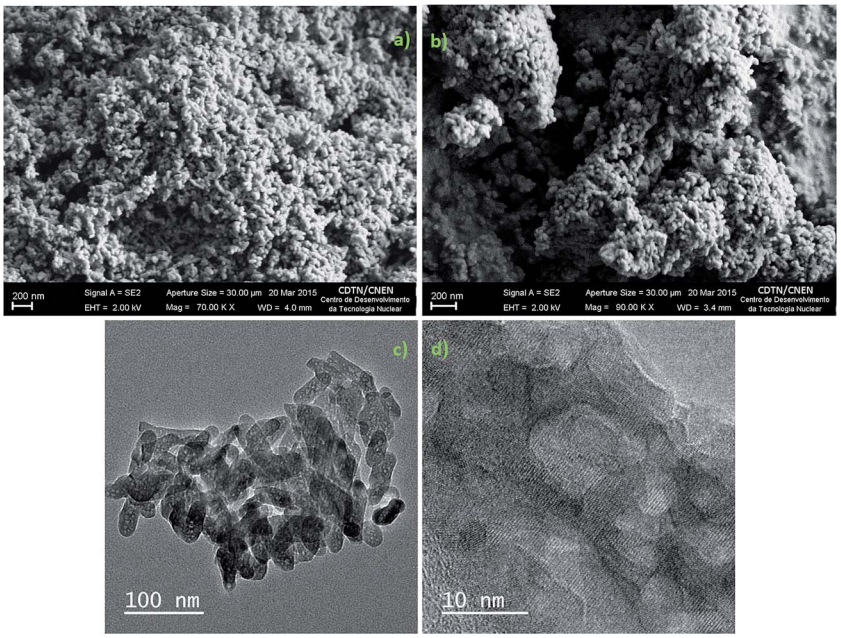

Fig. 10 SEM images of (a) HA and (b) HAThe functionalization strategy of HA with folate was tested. A systematic study of the structure and the chemical interaction were performed. The biocompatibility was also tested. HA–FA is a candidate to act as drug delivery or radioisotope carriers.–FA_{NH_2}; TEM image of (c) HA and (d) high resolution TEM image of HA.

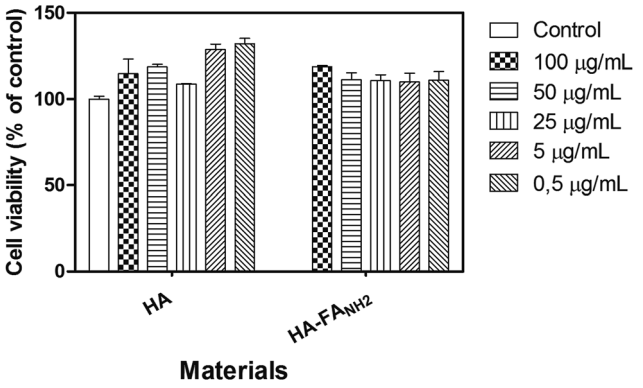

Fig. 12 Cell viability assay for biocompatibility.

Regarding these features, the synthesized hydroxyapatite and the functionalized sample showed great biocompatibility up to formulations at 100 μg mL^{-1} concentrations as seen on Fig. 12. Previous works found on the literature show that HA nanorods stimulate cell adhesion and proliferation,[34–39] explaining the cell viability above the control cells observed for all concentrations. Dry *et al.* (2013), Borowiec *et al.* (2014) and Lei Cai *et al.* (2014)[34,40,41] discussed the mechanisms involved in cell proliferation due to calcium ions concentrations on interstitial cell matrix, providing foundation to explain how HA could have this biological characteristics. Our proposal is that there is an exchange of ions between the hydroxyapatite matrix and the cellular environment triggering the mechanisms mentioned in these works. These results suggest that functionalized hydroxyapatite can facilitate bone tissue replacement after osteosarcoma treatment in a HA based drug delivery or radioisotopes carries systems, accrediting this material for the proposal of this work although more extensive biological tests must be necessary.

4 Conclusions

Based on XPS analyses and the other characterizations it is possible to assume that the functionalization process of hydroxyapatite nanorods with aminated folate, without using of a polymeric ligand or coating, can provide a very stable material with a strong interaction between hydroxyapatite nanorods surfaces and folate. This system is very important for osteosarcoma treatment since this kind of functionalization can allow active targeting of nanoparticles on tumor sites and make the cells recognize the hydroxyapatite surface as a biomaterial without reducing the bioactivity and osteoconductive effect, making possible to treat tumor cells and to promote bone tissue reconstruction. Moreover, the size range of the nanorods and its pore distribution make this system a promising agent to act in osteosarcoma treatment and diagnosis. As a radioisotope carrier system, folate can facilitate the internalization of hydroxyapatite nanorods and enhance the radiosensibility of this kind of tumor due to the proximity between cells nuclei and radiation source. These conclusions stimulate a deeper study of the biologic effects in osteosarcoma cells. As future works, our proposal is: (i) the investigation of *in vitro* adherence and internalization of these nanoparticles in SAOS-2 cells linage of human osteosarcoma in order to elucidate if the chemical interaction with hydroxyapatite nanorods does not interfere on folate capacity to recognize folic acid receptor, (ii) a deeper investigation on biocompatibility of these materials through more extensive *in vitro* cell viability assays on osteoblasts cells and (iii) an investigation on cytotoxicity of functionalized hydroxyapatite nanorods on SAOS-2 linage, especially when incorporated with radioisotopes.

Acknowledgements

This research was supported by the Brazilian agencies CAPES, CNPq and FAPEMIG. The authors would like to thank the Microscopy Center – UFMG for technical support during electron microscopy work.

References

1 A. Kolodziejczak-radzimska and M. Samuel, *Physicochem. Probl. Miner. Process.*, 2014, **50**(1), 225–236.
2 N. K. Nguyen, M. Leoni, D. Maniglio and C. Migliaresi, *J. Biomater. Appl.*, 2013, **28**, 49–61.
3 M. F. Cipreste and E. M. B. Sousa, *J. Biomater. Nanobiotechnol.*, 2014, **2014**, 24–30.
4 Z. Shi, X. Huang, B. Liu, H. Tao, Y. Cai and R. Tang, *J. Biomater. Appl.*, 2010, **25**, 19–37.
5 M. K. Yu, J. Park and S. Jon, *Theranostics*, 2012, **2**, 3–44.
6 V. Torchilin, *Adv. Drug Delivery Rev.*, 2011, **63**, 131–135.
7 S. Kuche Loghmani, M. Farrokhi-Rad and T. Shahrabi, *Ceram. Int.*, 2013, **39**, 7043–7051.
8 K. Watanabe, Y. Nishio, R. Makiura, A. Nakahira and C. Kojima, *Int. J. Pharm.*, 2013, **446**, 81–86.
9 B. Kundu, D. Ghosh, M. K. Sinha, P. S. Sen, V. K. Balla, N. Das and D. Basu, *Ceram. Int.*, 2013, **39**, 9557–9566.
10 K. Frederiksen, R. H. Guy and K. Petersson, *Eur. J. Pharm. Biopharm.*, 2015, **91**, 9–15.
11 R. Yang, E. A. Kolb, J. Qin, A. Chou, R. Sowers, B. Hoang, J. H. Healey, A. G. Huvos, P. a. Meyers and R. Gorlick, *Clin. Cancer Res.*, 2007, **13**, 2557–2567.
12 L. Treccani, T. Yvonne Klein, F. Meder, K. Pardun and K. Rezwan, *Acta Biomater.*, 2013, **9**, 7115–7150.
13 J. Pan, D. Wan, Y. Bian, H. Sun, C. Zhang, F. Jin, Z. Huang and J. Gong, *AIChE J.*, 2013, **59**, 4494–4501.
14 G. D. Venkatasubbu, S. Ramasamy, G. S. Avadhani, V. Ramakrishnan and J. Kumar, *Powder Technol.*, 2013, **235**, 437–442.
15 A. Ashokan, D. Menon, S. Nair and M. Koyakutty, *Biomaterials*, 2010, **31**, 2606–2616.
16 A. K. Sánchez Lafarga, F. P. Pacheco Moisés, A. Gurinov, G. G. Ortiz and G. G. Carbajal Arízaga, *Mater. Sci. Eng., C*, 2015, **48**, 541–547.
17 G. Verma, K. C. Barick, N. Manoj, A. K. Sahu and P. A. Hassan, *Ceram. Int.*, 2013, **39**, 8995–9002.
18 N. K. Nguyen, M. Leoni, D. Maniglio and C. Migliaresi, *J. Biomater. Appl.*, 2013, **28**, 49–61.

19 E. S. Lee, K. Na and Y. H. Bae, *J. Controlled Release*, 2003, **91**, 103–113.
20 T. Mosmann, *J. Immunol. Methods*, 1983, **65**, 55–63.
21 T. M. D. M. Martins, A. C. C. de Paula, D. A. Gomes and A. M. Goes, *Stem Cell Rev. Rep.*, 2014, **10**, 697–711.
22 F. Mohandes, M. Salavati-Niasari, Z. Fereshteh and M. Fathi, *Ceram. Int.*, 2014, **40**, 12227–12233.
23 W. P. S. L. Wijesinghe, M. M. M. G. P. G. Mantilaka, E. V. a. Premalal, H. M. T. U. Herath, S. Mahalingam, M. Edirisinghe, R. P. V. J. Rajapakse and R. M. G. Rajapakse, *Mater. Sci. Eng., C*, 2014, **42**, 83–90.
24 Q. Sun, J. Lou, F. Kang, J. Chen and J. Wang, *Powder Technol.*, 2014, **261**, 49–54.
25 M. Mir, F. L. Leite, P. S. d. P. Herrmann Junior, F. L. Pissetti, A. M. Rossi, E. L. Moreira and Y. P. Mascarenhas, *Mater. Res.*, 2012, **15**, 622–627.
26 N. Degirmenbasi, D. M. Kalyon and E. Birinci, *Colloids Surf., B*, 2006, **48**, 42–49.
27 J. d. S. R. Neto, *Hidroxiapatita sintética nanoestruturada e esmalte dental aquecidos e irradiados por laser de er,cr:ysgg: Caracterização por ftir e por drx*, Universidade de São Paulo, 2009.
28 S.-W. Tsai, J.-W. Liaw, F.-Y. Hsu, Y.-Y. Chen, M.-J. Lyu and M.-H. Yeh, *Sensors*, 2008, **8**, 6660–6673.
29 C. Sun, R. Sze and M. Zhang, *J. Biomed. Mater. Res., Part A*, 2006, **78**, 550–557.
30 S. Ferraris, S. Perero, E. Vern, E. Battistella, L. Rimondini and M. Ferraris, *Mater. Chem. Phys.*, 2011, **130**, 1307–1316.
31 C. Miot, E. Husson, C. Proust, R. Erre and J. Coutures, *J. Eur. Ceram. Soc.*, 1998, **18**, 339–343.
32 M. Kruk and M. Jaroniec, *Chem. Mater.*, 2001, **13**, 3169–3183.
33 L. C. M. Pinto, PhD thesis, Institute of Energy and Nuclear Research (IPEN), Sao Paulo University, Brazil, 1996.
34 L. Cai, A. S. Guinn and S. Wang, *Acta Biomater.*, 2011, **7**, 2185–2199.
35 L. Lin, R. Hao, W. Xiong and J. Zhong, *J. Biosci. Bioeng.*, 2014, 5–9.
36 S. Salehi and M. H. Fathi, *Ceram. Int.*, 2010, **36**, 1659–1667.
37 F. Qing, Z. Wang, Y. Hong, M. Liu, B. Guo, H. Luo and X. Zhang, *J. Mater. Sci.: Mater. Med.*, 2012, **23**, 2245–2251.
38 S. Agathopoulos, D. U. Tulyaganov, P. Valério and J. M. F. Ferreira, *Biomaterials*, 2005, **26**, 2255–2264.
39 Â. L. Andrade, P. Valério, A. M. Goes, M. De Fátima Leite and R. Z. Domingues, *J. Non-Cryst. Solids*, 2006, **352**, 3508–3511.
40 A. S. Borowiec, G. Bidaux, N. Pigat, V. Goffin, S. Bernichtein and T. Capiod, *Eur. J. Pharmacol.*, 2013, **739**, 19–25.
41 H. Dry, K. Jorgenson, W. Ando, D. a. Hart, C. B. Frank and A. Sen, *Cytotherapy*, 2013, **15**, 805–819.